

Quantification of Margins and Uncertainties for Integrated Spacecraft Systems Models

Thomas K. West IV* and Serhat Hosder†

Missouri University of Science and Technology, Rolla, Missouri 65409

and

Tyler Winter‡

M4 Engineering, Inc., Long Beach, California 90807

DOI: 10.2514/1.A33067

The objective of this study was to introduce an efficient and accurate approach to the quantification of margins and uncertainties for integrated spacecraft systems models. In this study, stochastic expansions, based on nonintrusive polynomial chaos, were used for efficient representation of uncertainty both in design metrics and associated performance limits of a system. Additionally, procedures were outlined for analyzing systems that contain different uncertainty types between the performance metrics and performance limits. These methodologies were demonstrated on two model problems, each possessing mixed (epistemic and aleatory) uncertainty, which was propagated through the models using second-order probability. The first was a complex system model of highly nonlinear analytical functions. The second was a coupled multisystem, physics-based model for spacecraft reentry. The performance metrics consisted of two systems used to determine the maximum g load, the necessary bank angle correction, and maximum convective heat load along a reentry trajectory. Overall, the methodologies and examples of this work have detailed an efficient approach for measuring the reliability of complex spacecraft systems models, as well as the importance of quantifying margins and uncertainties for the design of reliable systems.

Nomenclature

c_i	= mass fraction of species i	α	= deterministic coefficient in the polynomial chaos expansion
F	= performance metric	α^*	= generic uncertain function
FL, FU	= lower and upper performance limit	β	= confidence level
h	= enthalpy or altitude, km	γ	= flight-path angle, deg
h_D	= enthalpy of diffusion, J/kg	ϵ	= wall emissivity
h_0	= total enthalpy, J/kg	θ	= longitude, deg
h_f^0	= heat of formation, J/kg mol	μ	= dynamic viscosity, kg/m · s
Le	= Lewis number	ξ	= standard input random variable
M_{LW}, M_{UP}	= lower and upper performance gate margin	ρ	= density, kg/m ³
m	= mass, kg	σ	= Stefan-Boltzmann constant, 5.67×10^{-8} W/m ² ·K ⁴ , or bank angle, deg
N_s	= number of samples	ϕ	= latitude, deg
N_t	= number of terms in a total-order polynomial chaos expansion	Ψ	= random basis function or heading angle, deg
n	= number of random dimensions	ω	= planetary body rotation rate, rad/s
P	= pressure, Pa		
Pr	= Prandtl number		
p	= order of polynomial expansion		
\dot{q}	= heat flux, W/cm ²		
r	= orbital radius, km		
S	= reference area, m ²		
s	= downrange distance, km		
T	= temperature, K		
U	= velocity, m/s		
U_F	= performance metric uncertainty		
U_{FL}, U_{FU}	= lower and upper performance limit uncertainty		
U_{LW}, U_{UP}	= lower and upper performance gate uncertainty		

Subscripts

c	= conduction
d	= diffusion
e	= boundary-layer edge condition
r	= radiation
w	= wall condition
∞	= freestream condition

I. Introduction

IN COMPLEX aerospace engineering problems, reliability is a key component of the design process. Complex spacecraft systems and models may possess a significant amount of nondeterministic parameters and mission critical performance metrics that are subject to uncertainty. Quantifying this uncertainty, in not only designs, but also in performance limits, is critical in understanding and quantifying the reliability of a system. Because of the importance of such systems and associated models, there is a strong need for a simple, yet efficient and accurate approach to measure the confidence and reliability of complex spacecraft systems.

Quantification of margins and uncertainties (QMU) is a methodology developed to facilitate analysis and communication of confidence for certification of complex systems. This methodology is similar to the capability analysis reported in the past literature [1]. QMU is performed with quantified uncertainty and

Presented as Paper 2014-0682 at the AIAA SciTech 2014, National Harbor, MD, 13–17 January 2014; received 2 June 2014; revision received 17 August 2014; accepted for publication 18 September 2014; published online 5 January 2015. Copyright © 2014 by Thomas K. West IV, Serhat Hosder, and Tyler Winter. Published by the American Institute of Aeronautics and Astronautics, Inc., with permission. Copies of this paper may be made for personal or internal use, on condition that the copier pay the \$10.00 per-copy fee to the Copyright Clearance Center, Inc., 222 Rosewood Drive, Danvers, MA 01923; include the code 1533-6794/15 and \$10.00 in correspondence with the CCC.

*Graduate Student, Department of Mechanical and Aerospace Engineering, Student Member AIAA.

†Associate Professor of Aerospace Engineering, Department of Mechanical and Aerospace Engineering, Senior Member AIAA.

‡Aerospace Engineer, 4020 Long Beach Boulevard, Member AIAA.

margin metrics obtained for various system responses and performance parameters [2]. In recent years, a number of studies were reported on the theoretical development and the application of the QMU concept. The description of the key elements of a QMU framework was presented by Sharp and Wood-Schultz [2], who used the QMU methodology for the certification of nuclear weapons. Eardley [3] described QMU as a formalism dealing with the reliability of complex technical systems and the confidence, which can be placed in estimates of reliability. They also investigated the main components (performance gates, margins, and uncertainties) of QMU methodology. Pilch et al. [4] presented the main ideas underlying QMU, who also emphasized the need to separate aleatory and epistemic uncertainty in QMU. Helton [5] presented a comprehensive study on the QMU, which included a detailed analysis of the concept with different representations of uncertainty. Romero [6] discussed the issues and needs in QMU of complex coupled systems. Pepin et al. [7] presented a practical QMU metric for the certification of complex systems, which allowed uncertainty both on the operating region and the performance requirement and was not restrictive to a probabilistic definition of the uncertainty. A QMU approach was used for the characterization of the operational limits of the supersonic combustion engine of a hypersonic airbreathing vehicle by Iaccarino et al. [8]. A study by Lucas et al. [9] used the QMU methodology to study the reliability of a ring structure. Swiler et al. [10] studied various approaches to characterize epistemic uncertainty in the calculation of margins. Although significant work has been done in the area of QMU and its methodologies, further development of new methods is important for efficient, accurate, and comprehensive QMU for integrated spacecraft systems models.

The objectives of this work are twofold. The first objective is to demonstrate the use of stochastic response surfaces based on nonintrusive polynomial chaos (NIPC) for efficient quantification of uncertainty in system performance metrics, as well as performance boundaries. Previous work by Hosder and Bettis [11] and Bettis et al. [12], as well as Hosder et al. [13,14], in the area of using stochastic expansions based on NIPC as a means of efficient uncertainty quantification (UQ) has been extensively investigated. These works included studies involving the propagation of both aleatory (inherent) and epistemic uncertainties through a variety of stochastic model problems. In general, polynomial chaos methods are based on a spectral representation of the uncertainty and can be significantly more efficient than traditional Monte Carlo simulations. An additional advantage of NIPC methods is that the deterministic model, such as a computational fluid dynamics (CFD) code, is treated as a black box because no intrusive changes to the model are needed to perform UQ analyses. The theory behind the polynomial chaos methodologies are both well defined and well understood [15], making it a suitable and reliable method for UQ of complex spacecraft simulations and as a key component in an accurate and efficient QMU framework.

The second objective of this work is to define procedures to calculate the margin and uncertainty metrics for a QMU analysis of systems containing multiple types of uncertainty representation between the design and performance limits. In many engineering applications, uncertainty in the design condition may be different than the representation of the performance boundaries. Representation may be a pure probabilistic representation, an interval-based representation, or a combination of the two (i.e., mixed uncertainty). There may also be instances when no uncertainty exists in performance limits. This may be typical when trying to meet some specific design criteria. The goal is to outline how measures can be made between these different uncertainty representations to provide an accurate estimation of the reliability of the system and/or performance metric.

Methodologies developed in this study are demonstrated on two stochastic model problems. The first is an analytical model consisting of highly nonlinear functions typically used in optimization testing. This is to demonstrate the capability of NIPC when applied to complex problems and the use of stochastic response surfaces to represent uncertainty, as well as to demonstrate their use in a QMU

analysis. The analytical model or system has two performance metrics or outputs, each bounded by performance limits with a different uncertainty representation to demonstrate the aforementioned second objective of the current work. The second model problem is a multisystem, multiphysics spacecraft reentry model, which consists of coupled reentry dynamics and heat load models to characterize design critical measurements of a spacecraft during reentry. These include the maximum g load, the required bank angle correction, and the maximum heat load along the reentry trajectory. This model is intended to demonstrate the methodologies outlined in this work on a practical aerospace engineering application in the area of spacecraft systems.

The following section describes the methodology behind stochastic response surfaces using polynomial chaos expansions and their use as a means of accurate and efficient uncertainty quantification. Section III briefly describes the different types of uncertainty (aleatory and epistemic), as well as a short description of the process for propagating mixed uncertainty through a model. Section IV describes the formulation of the QMU methodologies and how the stochastic response surfaces can be incorporated into the analysis of systems with multiple types of uncertainty representation. The QMU methodologies are then demonstrated on a stochastic model consisting of highly nonlinear analytical functions (Sec. V) and a stochastic, multiphysics spacecraft reentry model (Sec. VI). These sections contain detailed information regarding the models, the stochastic problems, and the results of detailed QMU analyses. Lastly, conclusions summarizing the results are given to tie up the findings of this work.

II. Uncertainty Quantification Methodology

Many high-fidelity numerical models are computationally demanding. When performing UQ, traditional sampling methods may be problematic because large numbers of evaluations of the deterministic model are typically required for accurate results. In this study, a surrogate modeling approach based on polynomial chaos theory is used for improved computational efficiency. This section details the formulation of the surrogate models for use in accurate and efficient UQ.

In recent studies [11,12,14,16,17], the polynomial chaos method has been used as a means of UQ over traditional methods, such as Monte Carlo, for its computational efficiency. Polynomial chaos is a surrogate modeling technique based on the spectral representation of the uncertainty. An important aspect of spectral representations is the decomposition of a response value or random function α^* into separable deterministic and stochastic components, as shown in Eq. (1):

$$\alpha^*(\mathbf{x}, \xi) \approx \sum_{i=0}^P \alpha_i(\mathbf{x}) \Psi_i(\xi) \quad (1)$$

Here, α_i is the deterministic component and Ψ_i is the random variable basis functions corresponding to the i th mode; α^* is assumed to be a function of the vector \mathbf{x} of independent random variables and the n -dimensional standard random variable vector ξ . Note that this series is, by definition, an infinite series. However, in practice, it is truncated and a discrete sum is taken over a number of output modes [15]. To form a complete basis or for a total-order expansion, N_t terms are required, which can be computed from Eq. (2) for a polynomial chaos expansion (PCE) of order p and a number of random dimensions or variables n :

$$N_t = P + 1 = \frac{(n + p)!}{n! p!} \quad (2)$$

Further details on polynomial chaos theory are given by Eldred [15], Walters and Huyse [18], and Ghanem and Spanos [19].

The objective with any PCE method is to determine the expansion coefficients α_i . To do this, polynomial chaos methods can be implemented using an intrusive or a nonintrusive approach. Although

an intrusive method may appear straightforward in theory, for complex problems this process may be time consuming, expensive, and difficult to implement [11]. In contrast, the nonintrusive approach can be easily implemented to construct a surrogate model that represents a complex computational simulation, because no modification to the deterministic model is required. The nonintrusive methods require only the response (or sensitivity) [20–22] values at selected sample points to approximate the stochastic response surface.

Several methods have been developed for nonintrusive polynomial chaos. Of these, the point-collocation NIPC method has been used extensively in many aerospace simulations and CFD problems [12,14,17,20]. The point-collocation method starts with replacing a stochastic response or random function with its PCE using Eq. (1). Then, N_t vectors are chosen in random space and the deterministic code is then evaluated at these points, which is the left-hand side of Eq. (1). Following this, a linear system of N_t equations can be formulated and solved for the spectral modes of the random variables. This system is shown in Eq. (3):

$$\begin{pmatrix} \Psi_0(\xi_0) & \Psi_1(\xi_0) & \cdots & \Psi_P(\xi_0) \\ \Psi_0(\xi_1) & \Psi_1(\xi_1) & \cdots & \Psi_P(\xi_1) \\ \vdots & \vdots & \ddots & \vdots \\ \Psi_0(\xi_P) & \Psi_1(\xi_P) & \cdots & \Psi_P(\xi_P) \end{pmatrix} \begin{pmatrix} \alpha_0(x) \\ \alpha_1(x) \\ \vdots \\ \alpha_P(x) \end{pmatrix} = \begin{pmatrix} \alpha^*(x, \xi_0) \\ \alpha^*(x, \xi_1) \\ \vdots \\ \alpha^*(x, \xi_P) \end{pmatrix} \quad (3)$$

Note that, for this linear system, N_t is the minimum number of deterministic samples required to obtain an analytical solution (i.e., the coefficient vector). If more samples are available that are linearly independent, the system is considered overdetermined and can be solved using a least-squares approach. The number of samples over the required minimum is represented by the use of an oversampling ratio (OSR), defined as the ratio of number of actual samples to the minimum number required (i.e., N_t). In general, the number of collocation points can be determined by multiplying Eq. (2) by an OSR. Hosder et al. [13] determined an effective OSR of two for the stochastic model problems studied. It was shown that the accuracy of the PCE is dependent on the number of collocation points.

III. Types of Uncertainty and Mixed Uncertainty Propagation

A. Types of Uncertainty

Two main types of uncertainty exist in numerical modeling: aleatory uncertainty and epistemic uncertainty [23]. Aleatory uncertainty is the inherent variation of a physical system. Such variation is due the random nature of input data and can be mathematically represented by a probability density function if substantial experimental data are available for estimating the distribution type. An example of this for stochastic CFD simulations could be the fluctuation in freestream quantities. Although still considered a random variable, these variables are not controllable and their uncertainty is sometimes referred to as irreducible.

Epistemic uncertainty in a stochastic problem comes from several potential sources. These include a lack of knowledge or incomplete information of the behavior of a particular variable and ignorance or negligence with regard to accurate modeling of model parameters. Contrary to aleatory uncertainty, epistemic uncertainty is sometimes referred to as reducible uncertainty because an increase in knowledge regarding the physics of a problem, along with accurate modeling, can reduce the amount of this type of uncertainty. Epistemic uncertainty is typically modeled using intervals because the use of probabilistic distributions can lead to inaccurate predictions in the amount of uncertainty in a system. Upper and lower bounds of these intervals can be drawn from limited experimental data or from expert predictions and judgment [11,12].

An additional, special case of epistemic uncertainty is numerical error. This uncertainty is common in numerical modeling and is defined as a recognizable deficiency in any phase or activity of

modeling and simulations that is not due to lack of knowledge of the physical system. In CFD, an example of this type of uncertainty would be the discretization error in both the temporal and spatial domains that comes from the numerical solution of the partial differential equations that govern the system [12]. This uncertainty can be well understood and controlled through code verification and grid convergence studies.

B. Mixed Uncertainty Quantification

Many stochastic problems, including those to be used in this study, may contain both epistemic and aleatory types of uncertainty. It is desirable to consider the contribution of both types of uncertainty simultaneously by propagating this mixed uncertainty through the stochastic model. This can be done using a procedure known as second-order probability. The purpose of multistep UQ described in the preceding sections is to obtain an accurate NIPC response surface with computational efficiency. The NIPC response surface can then be used within second-order probability in place of the deterministic code, as shown in Fig. 1. Second-order probability is a type of double-loop sampling. In the outer loop, a vector of specific values for the epistemic variables is passed into the inner loop, where the stochastic response surface resulting from the NIPC process is sampled for the single epistemic sample vector and every aleatory sample vector. The process is repeated for all of the epistemic sample vectors. This means that the total number of samples of the NIPC response surface is the number of epistemic samples times the number of aleatory samples. Each iteration of the outer loop generates a cumulative distribution function based on the aleatory uncertainty analysis in the inner loop. After completion of the process, what remains is a series of CDFs, which, when plotted, gives intervals of the output variable from the model at different probability levels (i.e., P-box representation of mixed uncertainty output). This second-order probability can also be implemented with a Monte Carlo approach that uses the original model in the place of the response surface, which is done for the first model problem in this study for comparison with the NIPC results.

As shown by Eldred and Swiler [24], the outer (epistemic) loop may also be replaced by optimization-based interval size determination approaches, which include both local and global optimization methods to determine interval bounds of the output response at selected probability levels. In this work, an approach based on the combination of sampling and local optimization was used for the outer loop to determine the bounds at selected probability levels. The outer loop was first evaluated with a small number of samples to determine robust estimates for the initial values of epistemic variables used in local optimization. Then, the optimization is performed with these initial starting points for minimizing or maximizing the response at selected probability levels. This approach provides a computationally efficient means of obtaining accurate results (i.e., interval bounds) via optimization without the cost of performing large sampling on the response surface in the outer loop.

IV. Methodology for Quantification of Margins and Uncertainties

A. Components of QMU

The key measures in QMU are shown in Fig. 2. In this QMU framework, for the whole aerospace system (spacecraft or aircraft) or for each subsystem, the first step is to determine performance metrics

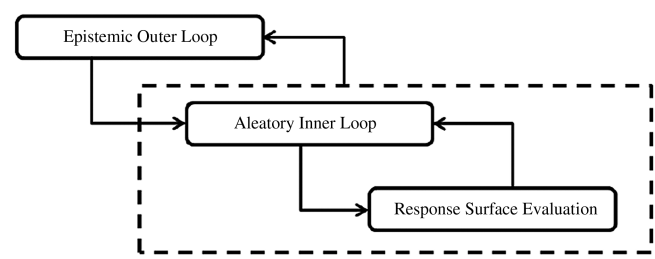


Fig. 1 Schematic of second-order probability.

(system outputs) relevant to the systems modeling. Then, these metrics are evaluated at a design condition (point) determined for safe and reliable operation of the aerospace system. Each of these metrics F typically involve some amount of uncertainty U_F due to the inherent (aleatory) or real-life variation of parameters used in physical models, as well as epistemic uncertainties. The safe and reliable operation region of the performance metrics (performance gates) may be bounded with a lower FL and/or an upper bound FU for each metric, which may also include some uncertainty (U_{FL} for FL and U_{FU} for FU) due to the aforementioned uncertainty sources. A measure of the distance between the design value of each performance metric and the lower boundary, including the effect of uncertainties U_F and U_{FL} , gives the lower margin U_{LW} and the distance between the upper boundary and the design value of each performance metric including the effect of uncertainties U_F and U_{FU} give the upper margin U_{UP} .

Using the uncertainty and the margin information, a metric has to be developed to quantify and certify the confidence in safe operation of a system with a given performance metric. A confidence ratio (CR) can be defined as shown in Eq. (4). The confidence ratio is obtained as the minimum of the ratio of the margin to the uncertainty calculated for each side of a performance metric. For a system wide confidence level, the minimum of the CRs is used to represent the most critical or unreliable component of the system. Note that a performance metric does not have to possess both an upper and a lower performance boundary. In fact, in many engineering applications, only a single limit may bound a performance metric. In this case, only a single ratio of the margin to the uncertainty exists and is considered as the confidence ratio for that particular metric (i.e., system performance or output):

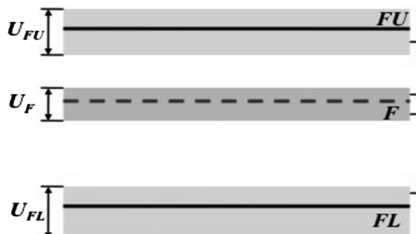
$$CR = \text{Min} \left[\frac{M_{UP}}{U_{UP}}, \frac{M_{LW}}{U_{LW}} \right] \quad (4)$$

B. Uncertainty Calculations

To measure the uncertainty in the performance gate(s) of a system, the first step is to perform the actual uncertainty quantification of the design and the performance limits. In many problems, stochastic models may be used for determining the uncertainty in the output based on random input variables. This can be done by various UQ propagation methods; however, it is one of the goals of the current study to use stochastic response surfaces for their computational efficiency and accuracy (see Sec. II). Also, models are not always directly available and the uncertainty must be quantified by other means. One example could be to use experimental test data. Then, it may be possible to represent the uncertainty of a design or performance limit with an interval or possibly fit a distribution to the data, depending on its behavior.

After quantifying the uncertainty in the design and the performance limits, the next step is to quantify the uncertainty in the performance gates. For a probabilistic representation of the uncertainty, one approach would be to use Eqs. (5) and (6):

$$U_{UP} = \sqrt{((FU_{max})_{P=0.5} - (FU_{min})_{P=\frac{1-\beta}{2}})^2 + ((F_{min})_{P=0.5} - (F_{max})_{P=\frac{1+\beta}{2}})^2} \quad (5)$$



U_{LW}

$$= \sqrt{((F_{max})_{P=0.5} - (F_{min})_{P=\frac{1-\beta}{2}})^2 + ((FL_{min})_{P=0.5} - (FL_{max})_{P=\frac{1+\beta}{2}})^2} \quad (6)$$

Here, β represents the confidence level used in the analysis and P represents the probability level at which the functional values are taken. For example, if $\beta = 0.95$, this would correspond to a 95% confidence level analysis. Note that, in these equations, the 50% probability level was selected such that approximately half of the uncertainty in the design and the limits is used to determine the uncertainty in the performance gate. This selection is used throughout this paper, but may be different depending on the application and the desired level of conservativeness. In case of mixed uncertainty in F , FU , and/or FL , min corresponds to the minimum and the max corresponds to maximum response value (bound) of the interval at that particular probability level, which can be obtained from the P box of the associated responses. Each of the square terms represent the uncertainty in either the design or a performance limit. Notice that the entire range of uncertainty in the design and the performance limits are not considered in Eqs. (5) and (6). By including only the uncertainty that will directly affect the performance gate on each side, the amount of uncertainty is restricted to each of the performance gates to avoid the underprediction of the reliability of the system. For example, the uncertainty in the upper performance gate is measured by roughly the upper half of the uncertainty in the design and the lower half of the uncertainty in the upper performance limit. Similarly, for the lower performance gate, the uncertainty is measured by roughly the lower half of the uncertainty in the design and the upper half of the uncertainty in the lower performance limit. In the case of mixed uncertainty, a conservative approach is taken to assess the amount of uncertainty in the performance gates. From Eq. (5), for example, the uncertainty in the design is measured as the distance between the upper output value at a selected probability level and the lower output value at the 50% probability level. Notice that the latter of the two values is taken further from the performance gate to ensure that any uncertainty that could affect the reliability of the system is included in the measurement of the amount of uncertainty in the performance limit.

The desired approach is to generalize the uncertainty measurements in Eqs. (5) and (6) to include nonprobabilistic representations of the uncertainty. This is done with Eqs. (7) and (8), in which each of the terms are defined, based on the representation of the uncertainty, in Tables 1 and 2 for the upper and lower performance gates, respectively:

$$U_{UP} = \sqrt{(U_{UP1} - U_{UP2})^2 + (U_{UP3} - U_{UP4})^2} \quad (7)$$

$$U_{LW} = \sqrt{(U_{LW1} - U_{LW2})^2 + (U_{LW3} - U_{LW4})^2} \quad (8)$$

C. Margin Calculations

Calculation of the distance between the design condition and the performance limit, or the margin, is a critical component of QMU. Improper measurement could result in under- or overprediction of the

- FU : Performance Upper Boundary
- U_{FU} : Uncertainty in FU
- F : Performance at Design Point
- U_F : Uncertainty in F
- FL : Performance Lower Boundary
- U_{FL} : Uncertainty in FL
- M_{UP} : Upper Margin
- M_{LW} : Lower Margin

Fig. 2 Schematic of key measures used in a QMU analysis.

Table 1 Response values of different uncertainty representations for upper uncertainty calculations

Uncertainty representation	U_{UP1}, FU	U_{UP2}, FU	U_{UP3}, F	U_{UP4}, F
No uncertainty	FU	FU	F	F
Pure epistemic	FU_{\max}	FU_{\min}	F_{\max}	F_{\min}
Pure aleatory	$(FU)_{P=0.5}^2$	$(FU)_{P=\frac{1-\beta}{2}}^2$	$(F)_{P=\frac{1-\beta}{2}}^2$	$(F)_{P=0.5}^2$
Mixed	$(FU_{\max})_{P=0.5}$	$(FU_{\min})_{P=\frac{1-\beta}{2}}$	$(F_{\max})_{P=\frac{1-\beta}{2}}$	$(F_{\min})_{P=0.5}$

Table 2 Response values of different uncertainty representations for lower uncertainty calculations

Uncertainty representation	U_{LW1}, FL	U_{LW2}, FL	U_{LW3}, F	U_{LW4}, F
No uncertainty	FL	FL	F	F
Pure epistemic	FL_{\max}	FL_{\min}	F_{\max}	F_{\min}
Pure aleatory	$(FL)_{P=0.5}^2$	$(FL)_{P=\frac{1+\beta}{2}}^2$	$(F)_{P=\frac{1-\beta}{2}}^2$	$(F)_{P=0.5}^2$
Mixed	$(FL_{\min})_{P=0.5}$	$(FL_{\max})_{P=\frac{1+\beta}{2}}$	$(F_{\min})_{P=\frac{1-\beta}{2}}$	$(F_{\max})_{P=0.5}$

reliability of the system. Although this measurement may graphically appear obvious, as seen in Fig. 2, if both the design and the performance limits possess uncertainty, the calculations should include the effects of these uncertainties to obtain an accurate margin estimate. Moreover, a general approach has been devised because the uncertainty characteristics (aleatory, epistemic, or mixed) for the design and limits may be different. Considering these, the calculation of the margins for a probabilistic representation of the uncertainty can be determined using Eqs. (9) and (10) for the upper and lower performance boundaries, respectively:

$$M_{UP} = |(FU_{\min})_{P=\frac{1-\beta}{2}} - (F_{\max})_{P=\frac{1+\beta}{2}}| \quad (9)$$

$$M_{LW} = |(F_{\min})_{P=\frac{1-\beta}{2}} - (FL_{\max})_{P=\frac{1+\beta}{2}}| \quad (10)$$

Here, β represents the confidence level used in the analysis and P represents the probability level at which the functional values are taken. For example, if $\beta = 0.95$, this would correspond to a 95% confidence level analysis.

If the distribution of the performance metric and/or the design limits are known (e.g., Gaussian), these values can be easily obtained from the statistics of the distribution. In general, the distribution of a system or model output is almost never known exactly, even when the inputs are on clearly defined distributions. In this case, response values may be obtained from a CDF formulation of the output. This is the typical approach when considering problems under a pure aleatory analysis or under mixed uncertainty where the outputs carry some probabilistic representation. Note also that the “min” and “max” subscripts in Eqs. (9) and (10) indicate the response value that should be selected when multiple response values exist at a single probability level. For instance, this occurs when a model or system is subject to mixed uncertainty as mentioned in Sec. III.B., which creates a range of values at each probability level defined by multiple CDFs (i.e., the CDFs that form the P box).

Another type of uncertainty representation of either the design or the limits may be the nonprobabilistic or pure epistemic representation. In this case, there is no distribution of the output and the uncertainty is only defined by an interval. Here the approach is to use the interval bounds as the measurement point for determining the margins rather than a response value defined at a specific probability level, which is not possible in this case. Note that this will be the most conservative approach and may be warranted given the unknown behavior of the uncertainty of epistemic intervals.

One of the objectives of this study is to demonstrate how a QMU analysis can be performed when the output uncertainty of design points and operational limits are different. The three possibilities

include pure epistemic (interval), pure aleatory, and mixed uncertainty. Equations (9) and (10) can be generalized to Eqs. (11) and (12), where each term is based on the representation of the uncertainty of the specific component of the system. The possible values of the M_{UP} and M_{LW} are summarized in Table 3:

$$M_{UP} = |M_{UP1} - M_{UP2}| \quad (11)$$

$$M_{LW} = |M_{LW1} - M_{LW2}| \quad (12)$$

V. Analytical QMU Model Problem

To demonstrate the quantification of margins and uncertainties using stochastic expansions with various uncertainty representation types in the design points and performance limits, an analytical model problem was selected. This model consists of a complex system of highly nonlinear functions typically used as test functions in numerical optimization studies. The objective with this model is to demonstrate both the UQ and QMU approaches described in the preceding sections on a general problem where two nonlinear systems are coupled, share common input variables, and both performance metrics and system boundaries have different uncertainty characteristics (i.e., pure aleatory, epistemic, or mixed). The following sections outline the deterministic model as well as the stochastic model. Then, both UQ and QMU are performed with a detailed description of the processes and the results.

A. Description of the Deterministic Model

1. Design

The deterministic model is shown in Fig. 3. This model consists of two primary systems including two outputs or performance metrics. Each system is made up of a nonlinear, analytical function. The first is the multivariate form of the Rosenbrock function and the second is known as the McCormick function. Notice also the dependence of system 2 on the output of system 1.

2. Performance Limits

The output of system 1 is constrained by both an upper and a lower performance limit. The upper limit is composed of its own model, shown in Eq. (13):

$$FU_1 = (y_1 + 2x_1 - 7)^2 + (2y_1 + x_1 - 5)^2 \quad (13)$$

This function is known as the Booth function. Notice that one of the variables in this function is the same as one of the variables in the system design. This adds a degree of complexity to the overall system. The lower limit is, however, not governed by a model, but rather is made up of statistical data. The second system is only bounded on the upper side. In this case, the uncertainty in the performance limit is represented by an epistemic interval.

B. Description of the Stochastic Model

1. Design

The design condition model consists of four input uncertain parameters. Two are represented by pure epistemic intervals and two

Table 3 Response values of different uncertainty representations for margin calculations

Uncertainty representation	M_{UP1}, FU	M_{UP2}, F	M_{LW1}, F	M_{LW2}, FL
No uncertainty	FU	F	F	FL
Pure epistemic	FU_{\min}	F_{\max}	F_{\min}	FL_{\max}
Pure aleatory	$(FU)_{P=\frac{1-\beta}{2}}$	$(F)_{P=\frac{1+\beta}{2}}$	$(F)_{P=\frac{1-\beta}{2}}$	$(FL)_{P=\frac{1+\beta}{2}}$
Mixed	$(FU_{\min})_{P=\frac{1-\beta}{2}}$	$(F_{\max})_{P=\frac{1+\beta}{2}}$	$(F_{\min})_{P=\frac{1-\beta}{2}}$	$(FL_{\max})_{P=\frac{1+\beta}{2}}$

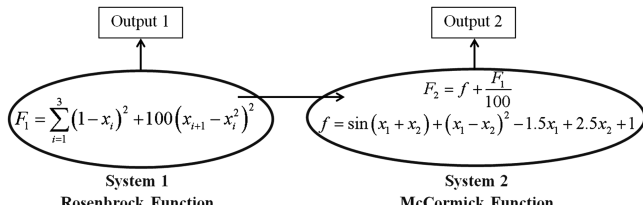


Fig. 3 System design schematic for the analytical model problem.

are aleatory variables with uniform distributions, indicating that the model design output (performance metric) will involve mixed uncertainty. These variables are shown in Table 4.

2. Performance Limits

As stated earlier, the upper boundary on the system 1 performance limits is defined by the model in Eq. (13). This model is made up of two uncertain variables, shown in Table 5. Notice again that one of the variables is the same as one from the design condition of the system.

The lower limit for system 1 is assumed to be made up of purely statistical data. These data are represented by a Gaussian distribution with a mean of -10.0 and a standard deviation of 0.1 . Lastly, the uncertainty in the upper limit of system 2 is represented by an epistemic interval given by $[15.0, 17.0]$. A summary of the performance limit uncertainty information is given in Table 5.

C. Uncertainty Quantification

1. Design

Performing the UQ on the performance metrics and the performance limits is the next step in the analysis. For system 1 of the design, a stochastic response surface could be formulated using a fourth-order polynomial chaos expansion. With four uncertain variables, a total number of 70 evaluations of the deterministic model were required using an OSR of two. The results are compared with a Monte Carlo (MC) simulation using the sampling/optimization approach in the epistemic loop of second-order probability described in Sec. III.B., which required 2074 evaluations of the deterministic model (optimization performed at 15 probability levels). The upper and lower CDFs of the output P box are given in Fig. 4, which also indicates the accuracy of the NIPC response surface when compared with MC.

For system 2 of the design, a stochastic response surface could be formulated using a fourth-order polynomial chaos expansion. With four uncertain variables, a total of 70 evaluations of the deterministic model were required using an OSR of two. The results are compared with a Monte Carlo simulation using the sampling/optimization approach in the epistemic loop of second-order probability described

Table 4 Uncertain input parameters for the analytical model performance metrics

Variable	Distribution	Mean/lower boundary	Standard deviation/upper boundary
x_1	Epistemic	-1.0	1.0
x_2	Uniform	-0.5	0.4
x_3	Uniform	-0.6	0.7
x_4	Epistemic	-0.5	1.0

Table 5 Uncertain input information for system 1 and system 2 performance limits

Variable	Distribution	Mean/lower boundary	Standard deviation/upper boundary
FU_1 input y_1	Gaussian	25.0	2.0
FU_1 input x_1	Epistemic	-1.0	1.0
FL_1	Gaussian	-10.0	0.1
FU_2	Epistemic	15.0	17.0

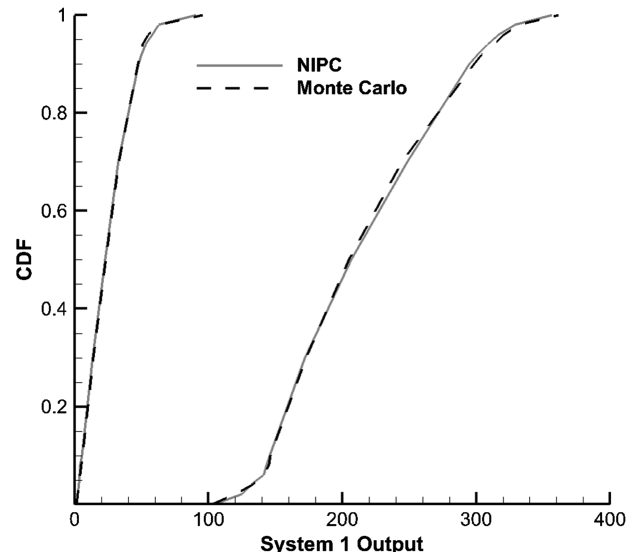


Fig. 4 System 1 output P -box plot.

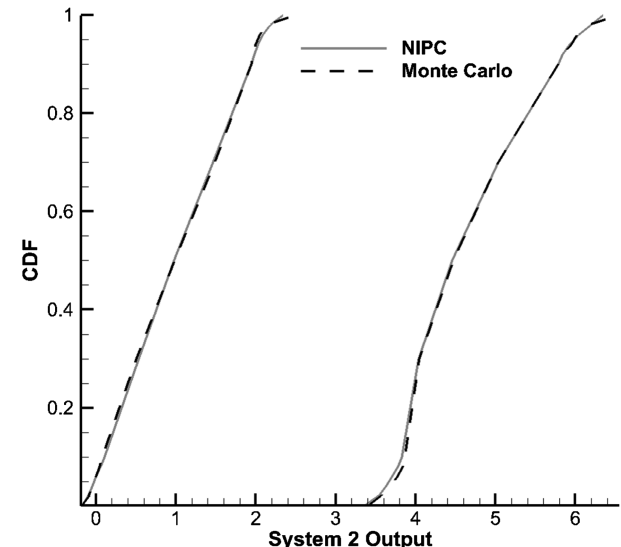


Fig. 5 System 2 output P -box plot.

in Sec. III.B., which required 1675 evaluations of the deterministic model (optimization performed at 15 probability levels). The upper and lower CDFs of the output P box are given in Fig. 5, which also shows a great agreement between NIPC and MC results.

2. Performance Limits

Similar to the design of the system, the uncertainty in the upper performance limit of system 1 was represented by a second-order polynomial chaos expansion. This required only 12 evaluations of the deterministic model using an OSR of two. A comparison with Monte Carlo is shown in Fig. 6 depicting the upper and lower CDFs of the output. Note that a total number of 61 evaluations of the deterministic model were required for the combined sampling/optimization Monte Carlo analysis (optimization performed at 15 probability levels).

The uncertainty in the two other performance limits are already specified because there is no model used to determine the output. For the lower performance limit of system 1, the uncertainty is represented by a Gaussian distribution with a mean of -10.0 and a standard deviation of 0.1 . The upper limit on system 2 is represented by an epistemic interval ranging from 15.0 to 17.0 .

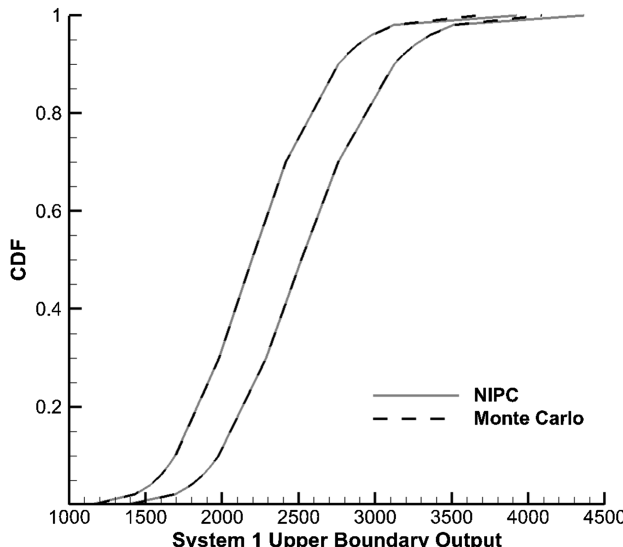


Fig. 6 P-box plot of the output of system 1 upper boundary.

D. Quantification of Margins and Uncertainties

After obtaining the uncertainty in the components of the system, the QMU analysis can be performed. A 95% confidence analysis (i.e., $\beta = 0.95$) has been selected for this problem. Using the equations and tables given in Sec. IV.B., the margin and performance gate uncertainty calculations can be performed. For system 1, both the design and the upper performance limit are represented by mixed uncertainty, whereas the lower limit is a pure aleatory representation. A summary of the margin and performance gate uncertainty values is given in Table 6, as well as the resulting confidence ratios of the system. Note that the minimum of these two confidence ratios is deemed the confidence ratio of system 1. The margin and uncertainty measurements are shown in Fig. 7. Note that the figures are not drawn to scale to increase the clarity.

Similarly, the QMU analysis is performed on system 2. Here, the design is represented by mixed uncertainty, whereas the only performance limit, located on the upper side of the performance metric, is represented by an epistemic interval. A summary of the system 2 QMU analysis metrics is as follows: upper performance gate, 8.84 margin, 5.28 uncertainty, and 1.67 confidence ratio.

There are two resulting confidence ratios from the QMU analysis, one from each system. A system-wide confidence level would then be the minimum of these two ratios, which is shown to be 0.057. This value indicates very poor confidence in the reliability of the system because the uncertainty in the performance gate between the design and the lower performance limit is significantly larger than the margin. From a practical standpoint, this would indicate that a reanalysis/design of the system, the performance limit, or both may be necessary to improve the reliability of the system.

VI. Spacecraft Reentry QMU Model Problem

To further demonstrate the quantification of margins and uncertainties using stochastic expansions with various uncertainty representations between the design points and performance limits, a second aerospace model problem is chosen, which is a multisystem physics-based model for atmospheric, lifting entry of a spacecraft. Systems within the design include a model for six-degree-of-freedom reentry dynamics used for the determination of a reentry trajectory.

Table 6 System 1 QMU analysis metrics

Performance gate	Margin	Uncertainty	CR
Lower	12.41	217.51	0.057
Upper	1119.65	1111.04	1.008

The second system is a prediction model of stagnation point, convective heat flux used to determine the maximum heat load experienced along the reentry trajectory. In this problem, a generic planetary entry capsule similar to the Crew Exploration Vehicle was analyzed for a lunar return mission [25–27]. The purpose of this model is to demonstrate the QMU of a coupled, multisystem design possessing mixed uncertainty, as well as performance boundaries with different types of uncertainty representation.

A. Description of the Deterministic Model

1. Design

The deterministic model is shown in the system diagram in Fig. 8. This model consists of two primary systems with three outputs or performance metrics.

The first system has two primary components or subsystems. The first of these is the trajectory model consisting of a six-degree-of-freedom model for atmospheric entry of a lifting body. The kinematics are shown in Eqs. (14–17) and the equations of the dynamic system are shown in Eqs. (18–20) [28,29]:

$$\frac{dr}{dt} = V \sin \gamma \quad (14)$$

$$\frac{d\phi}{dt} = \frac{V \cos \gamma \cos \psi}{r} \quad (15)$$

$$\frac{d\theta}{dt} = \frac{V \cos \gamma \sin \psi}{r \cos \phi} \quad (16)$$

$$\frac{ds}{dt} = V \cos \gamma \quad (17)$$

$$\frac{dV}{dt} = -\frac{D}{m} - g \sin \gamma + \omega^2 r \cos \phi (\sin \gamma \cos \phi - \cos \gamma \sin \phi \cos \psi) \quad (18)$$

$$V \frac{dy}{dt} = \frac{L}{m} \cos \sigma - g \cos \gamma + \frac{V^2}{r} \cos \gamma + 2\omega V \cos \phi \sin \psi + \omega^2 r \cos \phi (\cos \gamma \cos \phi + \sin \gamma \sin \phi \cos \psi) \quad (19)$$

$$V \frac{d\psi}{dt} = \frac{L \sin \sigma}{m \cos \gamma} + \frac{V^2}{r} \cos \gamma \sin \psi \tan \phi - 2\omega V (\tan \gamma \cos \phi \cos \psi - \sin \phi) + \frac{\omega^2 r}{\cos \gamma} \sin \phi \cos \phi \sin \psi \quad (20)$$

In this system, V is velocity, m is mass, D is drag, L is lift, r is the orbital radius, γ is the flight-path angle, θ is the longitude, ϕ is the latitude, σ is the bank angle, ω is the planetary body rotational speed, ψ is the heading angle, and s is the range. This is a system of seven ordinary differential equations that can be numerically integrated simultaneously in time. An example trajectory for a typical lunar return skip reentry mission is shown in Fig. 9.

The second component of this system is a guidance system, coupled to the primary reentry trajectory model. The guidance system is used to correct the trajectory in the instance of deviation from a nominal trajectory, such as when the reentry is subject to perturbation or uncertainty. To correct the trajectory, the guidance system uses a search algorithm to modify the bank angle of the trajectory. This effectively changes the direction of the lift vector to steer the spacecraft toward a target landing location. In this model problem, the reentry trajectory begins with the bank angle on the nominal value

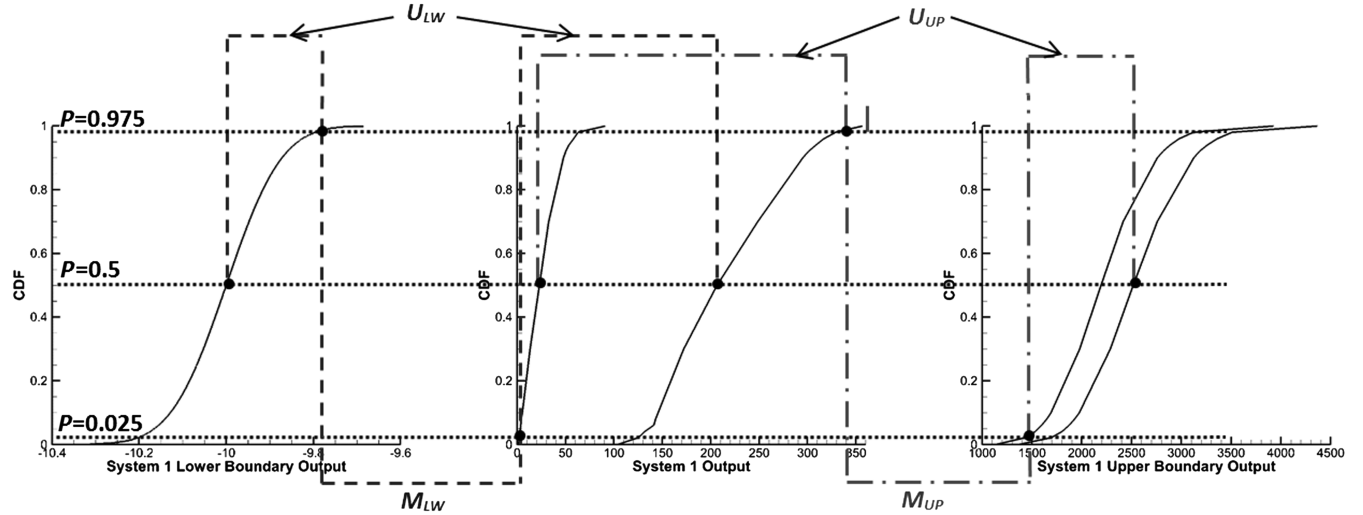


Fig. 7 QMU margin and uncertainty measurements for system 1 (not to scale).

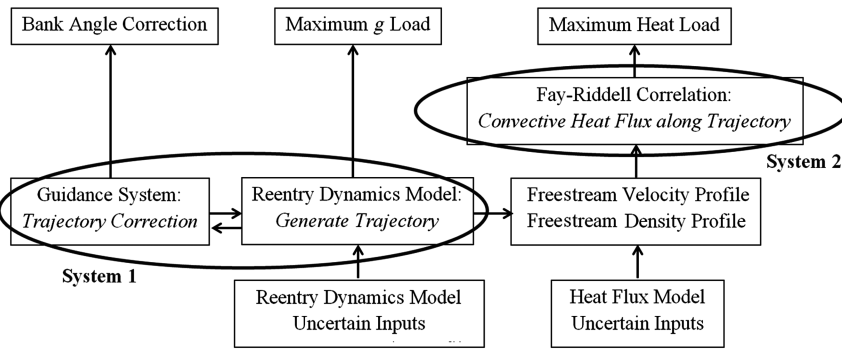


Fig. 8 System design schematic for the spacecraft reentry model problem.

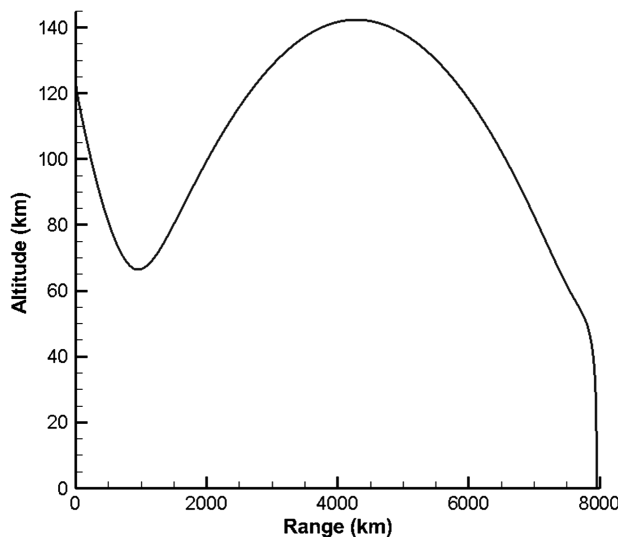


Fig. 9 Sample skip reentry trajectory.

for the baseline trajectory. A single bank angle correction is performed when a sensible atmosphere is detected, which occurs approximately when the g load reaches a value of 0.05 [30]. The necessary bank angle correction is determined using a simple root-finding method, shown in Eq. (21) for the i th step in the search. The search is based on the distance between the target location and the projected landing location at the current bank angle shown in Eq. (22), which is only a function of the bank angle because no other control is being simulated:

$$\sigma_i = \sigma_{i-1} - \frac{\sigma_{i-1} - \sigma_{i-2}}{f(\sigma_{i-1}) - f(\sigma_{i-2})} f(\sigma_{i-1}) \quad (21)$$

where

$$f(\sigma) = s_{\text{miss}} = s_{\text{current}} - s_{\text{target}} \quad (22)$$

Here, s_{current} is the range traveled with the current bank angle obtained from integrating the preceding dynamic system, and s_{target} is the range to the target from the current location measured as a greater circle distance. Once the optimum bank angle is determined, the baseline bank angle is corrected instantaneously and the remainder of the trajectory is carried out.

In the reentry dynamics system, there are a total of two outputs. The first is the maximum g load experienced along the trajectory. This is a critical trajectory and vehicle design value because it directly influences the safety of the crew as well as the structural loads that the vehicle may experience. The second output is the required bank angle correction. This value may be critical in the design of an adequate reaction control system including propulsive capabilities and propellant requirements [31].

The second system in this model is a model for the stagnation point convective heat flux of a blunt body in hypersonic flow. The Fay and Riddell [32] correlation was used to approximate the stagnation point heat transfer for a blunt body in hypersonic flow. This model assumes a laminar boundary layer, thermochemical equilibrium flow, and a fully catalytic wall. The model is shown in Eq. (23):

$$\dot{q}_w = 0.76(Pr^{-0.6})(\rho_w\mu_w)^{0.1}(\rho_e\mu_e)^{0.4} \sqrt{\frac{du_e}{dx}}(h_{0_e} - h_w) \times \left(1 + (Le^{0.52} - 1)\frac{h_D}{h_{0_e}}\right) \quad (23)$$

where

$$\frac{du_e}{dx} = \frac{1}{R_n} \sqrt{\frac{2(P_e - P_\infty)}{\rho_e}} \quad (24)$$

$$h_D = \sum_i c_i (h_f^0)_i \quad (25)$$

In the preceding equations, Pr is the Prandtl number, Le is the Lewis number, R_n is the radius of curvature of the body, h_D is the dissociation enthalpy, c_i is the mass fraction of the atomic species within the boundary layer, and $(h_f^0)_i$ is heat of formation of atomic species i . Note also that the subscripts w and e represent the wall and boundary-layer edge quantities, respectively. For this problem, a boundary condition at the wall is necessary to close the problem because fluid properties at the wall are required. A radiation, adiabatic wall condition was assumed. This implies that the wall temperature is not fixed, but the heat flux through the wall is zero (i.e., the heat transfer to the wall from the fluid due to conduction and diffusion must equal the heat transfer radiated away from the surface). Mathematically, this is shown with Eq. (26):

$$\dot{q}_r = \dot{q}_d + \dot{q}_c = \dot{q}_w \quad (26)$$

where

$$\dot{q}_r = \epsilon\sigma T_w^4 \quad (27)$$

Here, \dot{q}_d is the heat transfer due to diffusion, \dot{q}_c is the heat transfer due to conduction, ϵ is the wall emissivity, and σ is the Stefan–Boltzmann constant. Note that the heat transfer due to the radiation from the shock layer has been neglected. For given freestream conditions, the flow properties behind the standing bow shock along the stagnation streamline can be calculated using an equilibrium shock calculation procedure outlined in Anderson [33]. It can be assumed that the properties directly behind the shock are the properties on the edge of the boundary layer. The boundary-layer edge viscosity is calculated using Sutherland's law. The pressure at the wall can be assumed to be the pressure at the boundary-layer edge. Finally, the last step is to find the remaining properties at the wall; however, these are unknown because wall temperature is not specified. This requires then that Eqs. (23) and (26) be solved simultaneously with the system being implicitly dependent on the wall enthalpy (found using high-temperature equilibrium polynomial curve fits from Tannehill and Mugge [34]), wall viscosity (from Sutherland's law), and the wall density (from the equation of state). A simple root-finding method can be implemented to resolve the system. The solution of the system then gives the radiative, adiabatic wall temperature at which the convective heat flux to the wall is radiated away from the surface.

An important note should be made about the coupling between the reentry dynamics of system 1 and the aerothermodynamics of system 2. The heat flux is calculated at multiple points along the trajectory to locate the maximum value. Note that calculations are not performed when the continuum flow assumption is no longer valid (altitude greater than approximately 100 km) and when the flow is no longer supersonic. These conditions violate the assumptions of the model. However, the maximum heat flux would not occur in these regions, and so there is no possible loss of accuracy in capturing the maximum heat load.

2. Performance Limits

For system 1, performance limits exist for both outputs. The maximum g load is constrained by the limits the crew and the structure of the spacecraft can withstand, meaning that only an upper

limit exists. To represent this limit, an epistemic interval has been used. The performance limits of the bank angle correction would be based on the control and propellant limitations of the spacecraft. In this study, the upper and lower limits are firm boundaries, with no uncertainty. For system 2, there is only an upper limit on the heat flux because any lower limit would not be a concern. In this case, the upper limit was represented by an epistemic interval. This interval was selected to reflect the physical limitations of current thermal protection system materials.

B. Description of the Stochastic Model

1. Design

In system 1, there is a total of 10 uncertain variables, both coming from epistemic and aleatory sources. Epistemic sources include entry interface (EI) altitude, mass, drag coefficient, and lift coefficient. Aleatory sources include EI velocity, EI flight-path angle, the reference area, EI latitude, EI longitude, and EI heading angle. The uncertainty in these parameters and their distribution are shown in Table 7. Note that many of the selected uncertain parameters and classifications are consistent with previous uncertainty work in this area [25,26,28,29].

For system 2, 10 variables were selected as sources of uncertainty. Both epistemic (model form) and aleatory (inherent) forms of uncertainty were considered. The epistemic uncertain variables were as follows: Lewis number, Prandtl number, boundary-layer edge viscosity, emissivity, heats of formation for nitrogen and oxygen, and the power over the Lewis number. These model variables are considered as epistemic by imposing uncertainty on them due to lack of knowledge. Note that uncertainty in the two heats of formation and the boundary-layer edge viscosity were modeled through the introduction of a factor k to each variable, which was used to represent a variation in the uncertain variable [e.g., $x = k(x_{ref})$]. The factor k for each variable was treated as an epistemic uncertain variable. The other three variables were treated as aleatory (inherent) uncertain variables: freestream velocity, freestream density, and the radius of curvature of the body. Random fluctuations in the freestream conditions are possible during flight, and variations in the vehicle geometry are possible due to manufacturing processes. These variables were assumed normally distributed about some mean with a coefficient of variance of 1%. The input uncertainties for each of the uncertain variables are summarized in Table 8.

Table 7 Reentry model uncertain parameters for system 1

Variable	Distribution	Mean/minimum	Standard deviation/maximum
EI h , m	Epistemic	121,800	122,000
m , kg	Epistemic	9,000	9,500
C_D	Epistemic	1.27	1.31
C_L	Epistemic	0.367	0.407
EI U_∞ , m/s	Gaussian	10,900	30.0
EI γ , deg	Uniform	-6.1	-5.9
S , m^2	Gaussian	19.9	0.2
EI ϕ , deg	Gaussian	0.0	1.0
EI θ , deg	Gaussian	0.0	1.0
EI ψ , deg	Gaussian	0.0	1.0

Table 8 Reentry model uncertain parameters for system 2

Variable	Distribution	Mean/minimum	Standard deviation/maximum
Le	Epistemic	1.358	1.442
Pr	Epistemic	0.679	0.721
μ_e factor	Epistemic	0.97	1.03
ϵ	Epistemic	0.776	0.824
h_f^0 , N, Factor	Epistemic	0.97	1.03
h_f^0 , O, factor	Epistemic	0.97	1.03
Power on Le	Epistemic	0.5044	0.5356
U_∞ factor	Gaussian	1.0	0.01
ρ_∞ factor	Gaussian	1.0	0.01
R_n , m	Gaussian	6.93	0.0693

2. Performance Limits

For system 1, the upper performance limit is represented by an epistemic interval, as stated in the preceding section. The g -load limit was selected to be on the interval [10,11] g . Also for system 1, the limitations of the bank angle correction are defined as boundaries with no uncertainty. The boundaries were elected to be ± 20 deg. For system 2, the epistemic interval was selected to be [900, 1200] W/cm^2 . The uncertainty in this interval was extrapolated from several sources, indicating different heat load values of the Stardust mission, including CFD simulations as well as sensor data collected during flight [35–37].

C. Uncertainty Quantification

1. Design

Performing the UQ in the system design condition and the performance limits is the next step in the analysis. From the preceding section, there is a total of 20 uncertain parameters in this model problem. Using Eq. (2), 462 evaluations of the deterministic model were required for an OSR = 2 with second-order polynomial chaos expansions. The upper and lower CDFs of the output P boxes are given in Figs. 10 and 11 for the g load and bank angle correction, respectively. Note that these were obtained using the sampling approach for mixed uncertainty outlined in Sec. III.B..

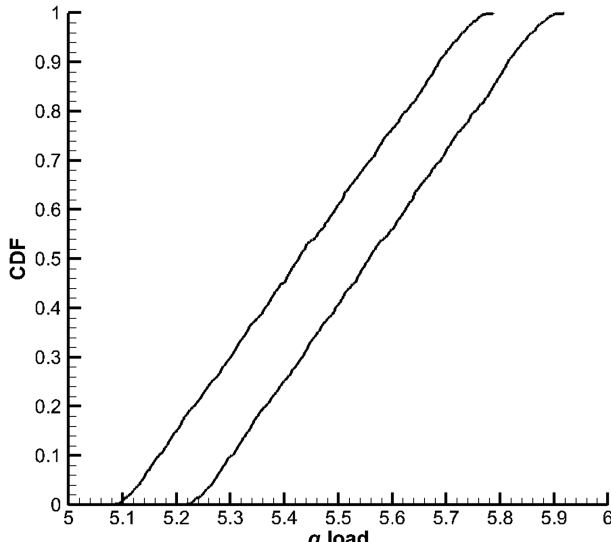


Fig. 10 Maximum g -load P -box plot from system 1.

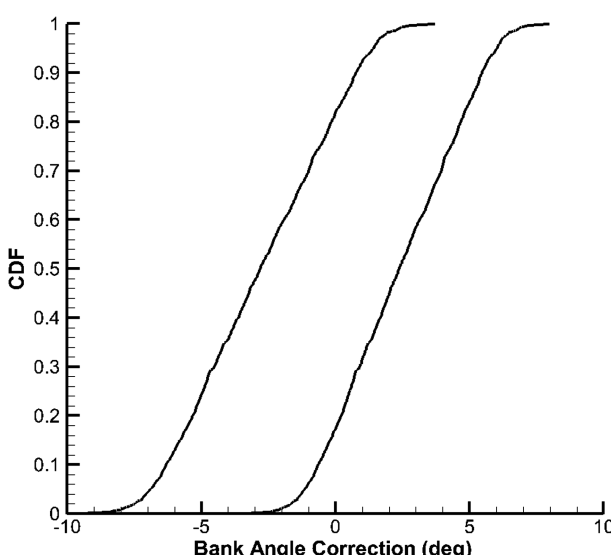


Fig. 11 Bank angle correction P -box plot from system 1.

A similar analysis was performed on system 2 of the design. A stochastic response surface could be formulated using a second-order polynomial chaos expansion. The upper and lower CDFs of the output P box are given in Fig. 12, which were obtained using the sampling approach for mixed uncertainty outlined in Sec. III.B..

In the previous model problem, a comparison of Monte Carlo and NIPC results was made to confirm the accuracy of the NIPC response surfaces. This was possible because of the low computational cost of the model. The reentry dynamics model is significantly more computationally expensive, making an accurate Monte Carlo solution infeasible to obtain. However, it is still possible to check the accuracy of the surrogate model by comparing results obtained from the actual model to those obtained from the surrogate model at the same sample location in the design space. In this study, 20 sample points, distributed evenly in the design space, were used to measure the accuracy of the surrogate models. Of the three surrogates created in this model problem, the highest mean error in the sample points was about 0.2%, validating the selection of second-order polynomial chaos expansions. Note that these sample points differ from the sample points used to train the surrogate model.

2. Performance Limits

No uncertainty quantification was performed on the performance limits for this model because both models were assigned epistemic intervals or boundaries with no uncertainty.

D. Quantification of Margins and Uncertainties

After assessing the uncertainty in the components of the system, the QMU analysis can be performed. A 95% confidence analysis (i.e., $\beta = 0.95$) has been selected for this problem. Using the equations and tables given in Sec. IV.B., the margin calculations can be performed. For system 1, both the design metrics are represented by mixed uncertainty. The upper performance limit of the maximum g load was represented by an epistemic interval, whereas the upper and lower bounds of the bank angle correction were fixed values with no uncertainty. A summary of the margin and performance gate uncertainty values, as well as the resulting confidence ratios of system 1 is given in Table 9 for the bank angle and as follows for the g -load: upper performance gate, 4.13 margin, 0.67 uncertainty, and 6.17 confidence ratio. Note that the minimum of these two confidence ratios is deemed the confidence ratio for the system.

Similarly, the QMU analysis is performed on system 2. Here, the design is represented by mixed uncertainty, whereas the only performance limit is represented by an epistemic interval. A summary of the margin and performance gate uncertainty values are as follows: upper performance gate, 775.92 margin, 150.98 uncertainty, and 5.14 confidence ratio.

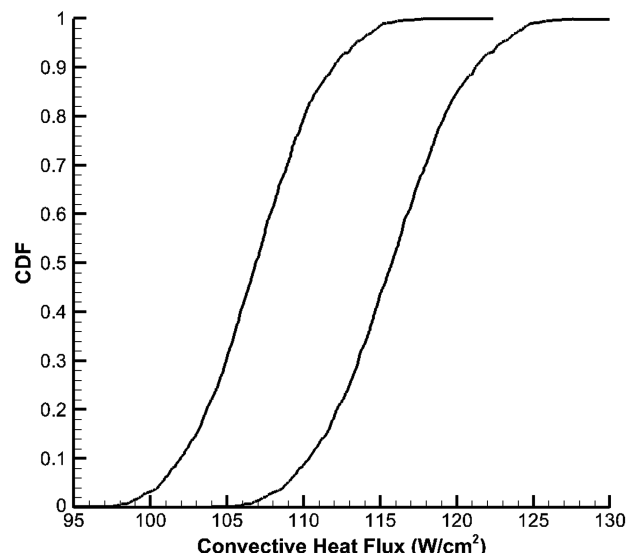


Fig. 12 Maximum heat load P -box plot from system 2.

Table 9 Bank angle correction QMU analysis metrics from system 1

Performance gate	Margin	Uncertainty	CR
Lower	12.61	9.77	1.29
Upper	13.67	9.14	1.50

There are two resulting confidence ratios from the QMU analysis, one from each system. A system-wide confidence level would then be the minimum of these three ratios, shown to be 1.29. This value indicates the weakest system in the design; however, in this case, the margins are greater than the uncertainty and the system design may be acceptable. If not, this would indicate that a reanalysis/design of the system, the performance limits, or both may be necessary to improve the reliability of the system.

VII. Conclusions

This study had two primary objectives for further advancement of the QMU methodologies implemented for integrated spacecraft systems models. The first objective was to demonstrate the use of stochastic expansions, based on nonintrusive polynomial chaos, to efficiently quantify the uncertainty in system design performance metrics, as well as performance boundaries. The second objective was to define procedures to measure margin and uncertainty metrics for QMU analysis of systems containing multiple types of uncertainty representation. To demonstrate the QMU methodologies developed in this work, two model problems were selected. These models contained design metrics and the performance limits, which included mixed (aleatory and epistemic) uncertainties.

The first model consisted of a complex system of highly nonlinear analytical functions typically used as test functions in numerical optimization studies. The objective with this model was to demonstrate both the uncertainty quantification using stochastic expansions and the QMU approaches on a general mathematical problem containing two coupled nonlinear systems that share common input variables. Additionally, both performance metrics and system boundaries have different uncertainty characteristics.

The second model was a coupled multisystem, multiphysics model of a spacecraft reentry. The design consisted of two physics-based systems possessing both epistemic and aleatory uncertainty. The first was a model for the reentry dynamics of a six-degree-of-freedom lifting body. The performance metrics of this system were the maximum g load experienced along the trajectory and the bank angle correction required to reach a target landing location. These are critical values in the design of a reentry system because it affects structural design of the spacecraft, the safety of any crew on board, and the design of the control system used during reentry. Performance boundaries were selected to reflect possible limitations of both performance metrics. The second system, which was coupled to the first, was a model for the stagnation point convective heat flux. Calculations were performed at multiple points along the trajectory to determine the maximum convective heat load experienced during reentry. The performance boundary of this metric was defined by current thermal protection material limitations and flight certifications.

Overall, the work done in this study has demonstrated a computationally efficient and accurate framework for the quantification of margins and uncertainties in complex spacecraft systems models. Procedures were outlined to treat various types of uncertainty representation in both performance metrics and performance limits. Multiple model problems, ranging in complexity, were used to not only demonstrate the methodologies presented in this work, but also to iterate the importance of accurate system reliability analysis.

Acknowledgments

Funding for this research was provided by NASA Jet Propulsion Laboratory under a Small Business Technology Transfer Phase II project grant NNX11CC60C (Lee D. Peterson, program manager).

References

- [1] *NIST/SEMATECH e-Handbook of Statistical Methods*, National Inst. of Standards and Technology, U.S. Dept. of Commerce, 2013.
- [2] Sharp, D. H., and Wood-Schultz, M. M., "QMU and Nuclear Weapons Certification. What's Under the Hood," *Los Alamos Science*, No. 28, 2003, pp. 47–53. <http://fas.org/sgp/othergov/doe/lanl/pubs/las28/sharp.pdf>
- [3] Eardley, D., "Quantification of Margins and Uncertainties (QMU)," EECS Dept., Univ. of California TR JSR-04-330, (JASON), Berkeley, CA, March 2005.
- [4] Pilch, M., Trucano, T. G., and Helton, J. C., "Ideas Underlying Quantification of Margins and Uncertainties (QMU): A White Paper," Sandia National Lab. Rept. SAND2006-5001, Albuquerque, NM, Sept. 2006.
- [5] Helton, J. C., "Conceptual and Computational Basis for the Quantification of Margins and Uncertainty," Sandia National Lab., Rept. SAND2009-3055, Albuquerque, NM, June 2009.
- [6] Romero, V. J., "Some Issues and Needs in Quantification of Margins and Uncertainty in Complex Coupled Systems," *47th AIAA/ASME/ASCE/AHS/ASC Structures, Structural Dynamics, and Materials Conference*, AIAA Paper 2006-1989, May 2006.
- [7] Pepin, J. E., Rutherford, A. C., and Hemez, F. M., "Defining a Practical QMU Metric," *49th AIAA/ASME/ASCE/AHS/ASC Structures, Structural Dynamics, and Materials Conference*, AIAA Paper 2008-1717, April 2008.
- [8] Iaccarino, G., Pecnik, R., Glimm, J., and Sharp, D., "QMU Approach for Characterizing the Operability Limits of Air-Breathing Hypersonic Vehicles," Los Alamos National Lab. Rept. LA-UR 09-01863, Los Alamos, NM, 2009.
- [9] Lucas, L. J., Owhadi, H., and Ortiz, M., "Rigorous Verification, Validation, Uncertainty Quantification and Certification Through Concentration-of-Measure Inequalities," *Computer Methods in Applied Mechanics and Engineering*, Vol. 197, Nos. 51–52, 2008, pp. 4591–4609. doi:10.1016/j.cma.2008.06.008
- [10] Swiler, L. P., Paez, T. L., Mayes, R. L., and Eldred, M. S., "Epistemic Uncertainty in the Calculation of Margins," *50th AIAA/ASME/ASCE/AHS/ASC Structures, Structural Dynamics, and Materials Conference*, AIAA Paper 2009-2249, May 2009.
- [11] Hosder, S., and Bettis, B., "Uncertainty and Sensitivity Analysis for Reentry Flows with Inherent and Model-Form Uncertainties," *Journal of Spacecraft and Rockets*, Vol. 49, No. 2, 2012, pp. 193–206. doi:10.2514/1.A32102
- [12] Bettis, B., Hosder, S., and Winter, T., "Efficient Uncertainty Quantification in Multidisciplinary Analysis of a Reusable Launch Vehicle," *17th AIAA International Space Planes and Hypersonic Systems and Technologies Conference*, AIAA Paper 2011-2393, April 2011.
- [13] Hosder, S., Walters, R. W., and Balch, M., "Efficient Sampling for Non-Intrusive Polynomial Chaos Applications with Multiple Uncertain Input Variables," *48th AIAA/ASME/ASCE/AHS/ASC Structures, Structural Dynamics, and Materials Conference*, AIAA Paper 2007-1939, April 2007.
- [14] Hosder, S., Walters, R. W., and Balch, M., "Point-Collocation Nonintrusive Polynomial Chaos Method for Stochastic Computational Fluid Dynamics," *AIAA Journal*, Vol. 48, No. 12, 2010, pp. 2721–2730. doi:10.2514/1.39389
- [15] Eldred, M. S., "Recent Advances in Non-Intrusive Polynomial Chaos and Stochastic Collocation Methods for Uncertainty Analysis and Design," *50th AIAA/ASME/ASCE/AHS/ASC Structures*, AIAA Paper 2009-2274, May 2009.
- [16] Witteveen, J. A. S., and Bijl, H., "Efficient Quantification of the Effect of Uncertainties in Advection Diffusion Problems Using Polynomial Chaos," *Numerical Heat Transfer*, Vol. 53, No. 5, 2008, pp. 437–465. doi:10.1080/10407790801960745
- [17] Han, D., and Hosder, S., "Inherent and Model-Form Uncertainty Analysis for CFD Simulation of Synthetic Jet Actuators," *48th AIAA Aerospace Sciences Meeting*, AIAA Paper 2012-0082, Jan. 2012.
- [18] Walters, R. W., and Huyse, L., "Uncertainty Analysis for Fluid Mechanics with Applications," NASA Langley Research Center, TR ICASE 2002-1, NASA CR-2002-211449, 2002.
- [19] Ghanem, R. G., and Spanos, P. D., *Stochastic Finite Elements: A Spectral Approach*, Springer-Verlag, New York, 1991.
- [20] West, T. K., IV, Hosder, S., and Johnston, C. O., "Multi-Step Uncertainty Quantification Approach Applied to Hypersonic Reentry Flows," *Journal of Spacecraft and Rockets*, Vol. 51, No. 1, 2014, pp. 296–310. doi:10.2514/1.A32592
- [21] Lockwood, B., and Mavriplis, D., "Gradient-Based Methods for Uncertainty Quantification in Hypersonic Flows," *Computers and Fluids Journal*, Vol. 85, Oct. 2013, pp. 27–38. doi:10.1016/j.compfluid.2012.09.003

[22] Roderick, O., Aniteescu, M., and Fischer, P., "Polynomial Regression Approaches Using Derivative Information for Uncertainty Quantification," *Nuclear Science and Engineering*, Vol. 164, No. 2, 2010, pp. 122–139.

[23] Oberkampf, W. L., Helton, J. C., and Sentz, K., "Mathematical Representation of Uncertainty," *Third Non-Deterministic Approaches Forum*, AIAA Paper 2001-1645, April 2001.

[24] Eldred, M., and Swiler, L., "Efficient Algorithms for Mixed Aleatory-Epistemic Uncertainty Quantification with Application to Radiation-Hardened Electronics," Sandia National Lab. Rept. SAND2009-5805, Albuquerque, NM, Sept. 2009.

[25] De Zaiacomo, G. M. K., Haya, R., and Penin, L. F., "Robust Skip Entry Guidance and Control for a Capsule Returning from Lunar Orbit," *AIAA Guidance, Navigation, and Control Conference*, AIAA Paper 2009-5771, Aug. 2009.

[26] Hoelscher, B., "Orion Entry, Descent, and Landing," *AIAA Guidance, Navigation, and Control Conference*, AIAA Paper 2007-6428, Aug. 2007.

[27] Berger, K., "Aerothermodynamic Testing of the Crew Exploration Vehicle in the LaRC 20-Inch Mach 6 and 31-Inch Mach 10 Tunnels," *46th AIAA Aerospace Sciences Meeting*, AIAA Paper 2008-1225, Jan. 2008.

[28] Xue, S., and Lu, P., "Constrained Predictor-Corrector Entry Guidance," *Journal of Guidance, Control, and Dynamics*, Vol. 33, No. 4, 2010, pp. 1273–1281.
doi:10.2514/1.49557

[29] Brunner, C., and Lu, P., "Skip Entry Trajectory Planning and Guidance," *AIAA Guidance, Navigation, and Control Conference*, AIAA Paper 2007-6777, Aug. 2007.

[30] D'Souza, S., and Sarigul-Klijn, N., "Investigation of Trajectory Generation for a Mission Adaptive Planetary Entry Guidance Algorithm," *AIAA Atmospheric Flight Mechanics Conference*, AIAA Paper 2012-4508, Aug. 2012.

[31] Hoelscher, B. R., Strahan, A. L., Stachowiak, S. J., and Loe, G. R., "Orion Entry Flight Control Modifications and Performance," *AIAA Guidance, Navigation, and Control Conference*, AIAA Paper 2008-7152, Aug. 2008.

[32] Fay, J. A., and Riddell, F. R., "Theory of Stagnation Point Heat Transfer in Dissociated Air," *Journal of the Aeronautical Sciences*, Vol. 25, No. 2, 1958, pp. 73–85.
doi:10.2514/8.7517

[33] Anderson, J. D. Jr., *Hypersonic and High-Temperature Gas Dynamics*, 2nd ed., AIAA, Reston, VA, 2006, pp. 604–606.

[34] Tannehill, J. C., and Mugge, P. H., "Improved Curve Fits for the Thermodynamic Properties of Equilibrium Air Suitable for Numerical Computation Using Time-Dependent or Shock-Capturing Methods," NASA CR-2470, Oct. 1974.

[35] Trumble, K., Cozmuta, I., Sepka, S., Jenniskens, P., and Winter, M., "Postflight Aerothermal Analysis of Stardust Sample Return Capsule," *Journal of Spacecraft and Rockets*, Vol. 47, No. 5, 2010, pp. 765–774.
doi:10.2514/1.41514

[36] Chen, Y., Squire, T., Laub, B., and Wright, M., "Monte Carlo Analysis for Thermal Protection System Design," *Ninth AIAA/ASME Joint Thermophysics and Heat Transfer Conference*, AIAA Paper 2006-2951, June 2006.

[37] Shang, J., and Surzhikov, T., "Simulating Stardust Earth Reentry with Radiation Heat Transfer," *Journal of Spacecraft and Rockets*, Vol. 48, No. 3, 2011, pp. 385–396.
doi:10.2514/1.52029

G. Palmer
Associate Editor